

ProtoHPE: Prototype-guided High-frequency Patch Enhancement for Visible-Infrared Person Re-identification

Guiwei Zhang
Beijing Key Laboratory of Digital Media, School of Computer Science and Engineering, Beihang University, Beijing, China
zhangguiwei@buaa.edu.cn

Yongfei Zhang*
Beijing Key Laboratory of Digital Media, State Key Laboratory of Virtual Reality Technology and Systems, School of Computer Science and Engineering, Beihang University, Beijing, China
yfzhang@buaa.edu.cn

Zichang Tan
Department of Computer Vision Technology (VIS), Baidu Inc. Beijing, China
tanzichang@baidu.com

ABSTRACT

Visible-Infrared person re-identification is challenging due to the large modality gap. To bridge the gap, most studies heavily rely on the correlation of visible-infrared holistic person images, which may perform poorly under severe distribution shifts. In contrast, we find that some cross-modal correlated high-frequency components contain discriminative visual patterns and are less affected by variations such as wavelength, pose, and background clutter than holistic images. Therefore, we are motivated to bridge the modality gap based on such high-frequency components, and propose **Prototype-guided High-frequency Patch Enhancement (ProtoHPE)** with two core designs. **First**, to enhance the representation ability of cross-modal correlated high-frequency components, we split patches with such components by Wavelet Transform and exponential moving average Vision Transformer (ViT), then empower ViT to take the split patches as auxiliary input. **Second**, to obtain semantically compact and discriminative high-frequency representations of the same identity, we propose Multimodal Prototypical Contrast. To be specific, it hierarchically captures comprehensive semantics of different modal instances, facilitating the aggregation of high-frequency representations belonging to the same identity. With it, ViT can capture key high-frequency components during inference without relying on ProtoHPE, thus bringing no extra complexity. Extensive experiments validate the effectiveness of ProtoHPE.

CCS CONCEPTS

• Computing methodologies → Artificial intelligence.

KEYWORDS

VI-ReID, high-frequency enhancement, prototypical contrast

*Corresponding author.

Permission to make digital or hard copies of all or part of this work for personal or classroom use is granted without fee provided that copies are not made or distributed for profit or commercial advantage and that copies bear this notice and the full citation on the first page. Copyrights for components of this work owned by others than the author(s) must be honored. Abstracting with credit is permitted. To copy otherwise, or republish, to post on servers or to redistribute to lists, requires prior specific permission and/or a fee. Request permissions from permissions@acm.org.

MM '23, October 29–November 3, 2023, Ottawa, ON, Canada

© 2023 Copyright held by the owner/author(s). Publication rights licensed to ACM.

ACM ISBN 979-8-4007-0108-5/23/10...\$15.00

<https://doi.org/10.1145/3581783.3612297>

ACM Reference Format:

Guiwei Zhang, Yongfei Zhang, and Zichang Tan. 2023. ProtoHPE: Prototype-guided High-frequency Patch Enhancement for Visible-Infrared Person Re-identification. In *Proceedings of the 31st ACM International Conference on Multimedia (MM '23)*, October 29–November 3, 2023, Ottawa, ON, Canada. ACM, New York, NY, USA, 12 pages. <https://doi.org/10.1145/3581783.3612297>

1 INTRODUCTION

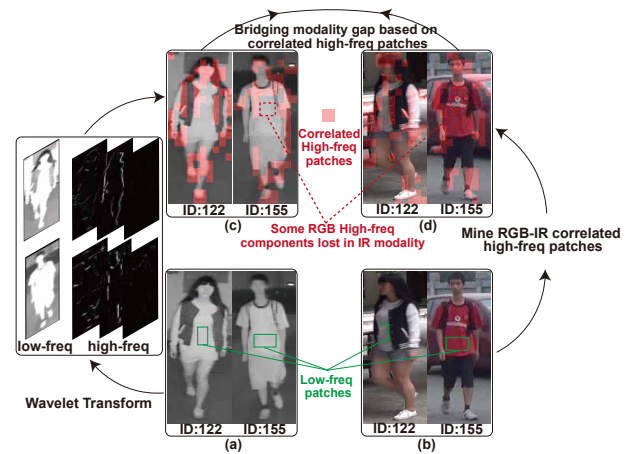


Figure 1: Illustration of our idea. (a) and (b) are holistic IR and RGB images, respectively. In (c) and (d), some RGB-IR correlated high-frequency patches contain discriminative visual patterns, e.g., heads, cloth textures, and human silhouettes. Such patches are less affected by variations such as wavelength, pose, and background clutter than holistic images, and thereby are more robust to distribution shifts. We are thus motivated to bridge the gap based on these patches.

Person re-identification (ReID) aims to retrieve a specific person, given in a query image, from non-overlapping camera views [43, 48, 49]. Most research to date has focused on RGB cameras [19, 30, 45, 52]. However, RGB cameras perform poorly in capturing the appearance of people in low-light conditions. In contrast, near-infrared (IR) cameras can remedy such inadequacy of RGB cameras due to their robustness to illumination variations. Hence, visible-infrared ReID (VI-ReID) has recently attracted great attention. Specifically,

VI-ReID aims to retrieve a person, given in an IR query, from the search over RGB person images and vice versa [32, 43].

VI-ReID is challenging due to the large modality gap. To bridge the gap, most existing methods focus on learning modality-shared and modality-compensated feature representations [20, 23, 51]. However, these methods heavily rely on the correlation of RGB and IR holistic person images and may perform poorly under severe distribution shifts. Such distribution shifts are common in VI-ReID due to large differences in wavelength, scattering, pose, and background clutter between person images of different modalities. This issue was still understudied in previous VI-ReID works, thus resulting in poor performance in bridging the modality gap.

To this end, we explore a more suitable solution to bridge the modality gap from a frequency perspective, which is of great significance in digital image processing [14, 26, 27, 39, 45]. In Fig. 1, we first utilize Haar Wavelet Transform to decompose IR person images into low- and high-freq components, and then select patches with top- K high-freq responses, termed IR high-freq patches.¹ Please note that we directly define the high-freq responses as the l_2 -norm of high-freq components of person images (Section 4.1). We compare the selected patches above and reveal:

(1) IR high-freq patches contain more discriminative visual patterns than IR low-freq patches. From Fig. 1 (a), due to longer wavelength and more scattering than visible light, visually similar IR low-freq patches can represent different semantics, e.g., visual patterns of white and red shirts in Fig. 1 (b). Enhancing such patches may cause feature representations to lose identity discrimination. In contrast, IR high-freq patches contain more discriminative visual patterns, e.g., heads, certain cloth textures, and human silhouettes in Fig. 1 (c), and thus are more critical components to boost VI-ReID.

(2) The modality gap between RGB-IR correlated high-freq patches is much smaller than that between holistic images. From Fig. 1 (c) and (d), although some RGB high-freq components are lost in the IR modality due to large differences in wavelength and scattering between two modalities, there are always RGB patches highly correlated with IR high-freq patches. Such RGB-IR correlated high-freq patches contain discriminative visual patterns that are less affected by variations such as wavelengths, pose, and background clutter than holistic images, and thereby are more robust to the distribution shift. We are thus motivated to bridge the modality gap based on RGB-IR correlated high-freq patches effectively.

However, previous VI-ReID methods [23, 24, 34] only bridge the modality gap by optimizing instance representations in the mini-batch, which may cause inconsistent representations of the same identity in different mini-batches. To address this issue, recent research proposes cross-modal instance-prototype contrast [4], in which a prototype is defined as a representative embedding for a group of semantically similar instances. Despite progress, this contrastive approach ignores direct semantic constraints between different modal prototypes. Since prototypes can characterize the joint distribution of multiple modalities in a compact form, we argue that enforcing direct semantic constraints between prototypes facilitates stable interactions between structural distributions of

different modalities. This is beneficial to extract more compact and informative representations, which improves robustness to the gap.

In summary, the key to our idea lies in two points: capturing RGB-IR correlated high-freq patches, and robustly bridging the modality gap based on these patches. To this end, we propose **Prototype-guided High-freq Patch Enhancement (ProtoHPE)** with two core designs. **First**, we propose Cross-modal High-freq Patch Enhancement (Section 4.1), in which Haar Wavelet Transform and exponential moving average Vision Transformer (ViT) [11] are jointly utilized to mine RGB-IR correlated high-freq patches. Such patches are then fed into ViT as auxiliary input to enhance the representation ability of RGB-IR correlated high-freq components. **Second**, to obtain semantically compact and discriminative high-freq representations of the same identity during network optimization, we propose Multimodal Prototypical Contrast (MultiProCo). Note that a modality prototype is defined as a representative embedding for instances belonging to the same identity and the same modality. MultiProCo (Section 4.2) captures comprehensive semantics of different modal instances in a hierarchical manner, where lower-level *instance-prototype constraint* captures the semantics of instances within a modality belonging to the same identity, while higher-level *multimodal prototypes contrastive regularization* captures structural distributions across different modalities and different identities. This facilitates the aggregation of high-freq enhanced representations belonging to the same identity, which helps to learn compact and discriminative representations to robustly bridge the gap. With MultiProCo, ViT can capture key high-freq components during inference without relying on ProtoHPE, thus bringing no extra complexity. Our contributions include:

- We propose Cross-modal High-freq Patch Enhancement to enhance the representation ability of RGB-IR correlated high-freq patches. Bridging the modality gap based on these patches is more robust to the distribution shift compared to holistic images.
- We propose Multimodal Prototypical Contrast, which hierarchically captures comprehensive semantics of different modal instances. It facilitates the aggregation of high-freq enhanced representations belonging to the same identity, thus bridging the modality gap robustly. With it, ViT can capture key high-freq components during inference without relying on ProtoHPE, bringing no extra complexity.
- Extensive experimental results perform favorably against mainstream methods on SYSU-MM01 and RegDB datasets.

2 RELATED WORK

2.1 Visible-Infrared Person Re-identification

Visible-Infrared person Re-identification is challenging due to the large cross-modal gap. To bridge the gap, existing schemes can be roughly summarized into the following two aspects.

(1) Some works mitigate the large modality discrepancy by introducing generation-based methods [9, 31, 33?]. AlignGAN [31] exploits pixel- and feature-level alignment jointly to alleviate the cross-modal variations. D²RL [33] mitigates the modality discrepancy by generating multi-spectral images with a bi-directional cycle GAN. XIV [?] generates an auxiliary X-modality to bridge the visible and infrared modalities.

¹For simplicity, we abbreviate “low-frequency” and “high-frequency” as “low-freq” and “high-freq”, respectively, in this paper.

(2) Others develop various dual-stream networks to learn modal-shared and modal-compensated features [13, 15, 23, 24, 40, 42, 46, 51]. MACE [40] proposes a sharable two-stream network to alleviate the modality gap in both feature and classifier levels. MSO [15] proposes edge features enhancement to enhance modality-sharable features. CM-NAS [13] proposes BN-oriented search architecture to boost cross-modal matching. cm-SSFT [24] explores the potential of both modality-shared and modality-specific features to boost performance. MSCLNet [51] synergizes and complements instances of different modalities to learn discriminative representations. CMT [20] introduces a Transformer encoder-decoder design to compensate for the missing modality-specific information.

Despite inspiring progress, the above approaches heavily rely on the correlation of RGB-IR holistic person images and may perform poorly under severe distribution shifts. In contrast, we bridge the modality gap based on RGB-IR correlated high-freq patches, which are more robust to distribution shifts than holistic images.

2.2 Self-supervised Learning

Self-supervised learning (SSL) for vision aims to learn general-purpose representations without human supervision [12]. Since SimCLR [5] demonstrated effectiveness on the instance-level discrimination task, contrastive learning has dominated the state-of-the-art SSL models [2, 7, 21]. However, SimLCR heavily relies on sufficient negatives in the mini-batch. To tackle this issue, MoCo [17] introduces a dynamic dictionary with a queue and SimSiam [6] learns meaningful representations without negative sample pairs.

Recently, the success of contrastive learning has inspired the generalization of this method to Contrastive Language Image Pretraining (CLIP) [29], where images and texts are considered as multimodal views of the same underlying concepts. X-CLIP [25] focuses on multi-grained contrastive learning for accurate cross-modal alignment. ProtoCLIP [4] sets up instance-prototype discrimination, which efficiently transfers higher-level structural knowledge in vision-language pretraining. Progressive self-distillation [1] learns robust representations from noisy data to boost cross-modal contrastive learning.

However, the above approaches neglect direct semantic constraints between different modal prototypes. Since prototypes can characterize the joint distribution of multiple modalities in a compact form, imposing direct semantic constraints between prototypes helps to capture structural distributions of different modalities. Therefore, we propose multimodal prototypical contrast, which hierarchically captures comprehensive semantics of different modal instances. This facilitates learning compact and discriminative representations, which improves robustness to the modality gap.

3 PRELIMINARIES

3.1 Part-based ViT Baseline.

Given a RGB/IR person image, we split it into N patches $\{x_i | i = 1, 2, \dots, N\}$ and tokenize them with learnable linear projection \mathcal{F} and position embeddings $E_{\text{pos}} \in \mathbb{R}^{(1+N) \times D}$, such that

$$\mathbf{X} = [\mathbf{x}_{[\text{CLS}]}, \mathcal{F}(\mathbf{x}_1), \mathcal{F}(\mathbf{x}_2), \dots, \mathcal{F}(\mathbf{x}_N)] + E_{\text{pos}} \quad (1)$$

where $\mathbf{X} \in \mathbb{R}^{(1+N) \times D}$ denotes the input sequence and $\mathbf{x}_{[\text{CLS}]}$ is a learnable class token. We take \mathbf{X} as input to a sequence of l transformer blocks, and the hidden output of the l -th block is denoted by \mathbf{h}_l . Subsequently, all embeddings in \mathbf{h}_l except the class token $\mathbf{x}_{[\text{CLS}]}$ are divided into T parts uniformly. Then, T parts that concatenate $\mathbf{x}_{[\text{CLS}]}$ are further fed into a shared Transformer block to extract T local part representations $\{f_j | j = 1, 2, \dots, T\}$, in which f_j is the encoded class token of the j -th part. Furthermore, a global Transformer block operates on the hidden output \mathbf{h}_l , and the encoded class token is served as the global representation f_g . By convention, we optimize the representations f_g and $\{f_j | j = 1, 2, \dots, T\}$ with the cross-entropy loss \mathcal{L}_{CE} and the triplet loss \mathcal{L}_{Tri} , respectively:

$$\mathcal{L}_{base} = \mathcal{L}_{CE}(f_g) + \mathcal{L}_{Tri}(f_g) + \frac{1}{T} \sum_{j=1}^T (\mathcal{L}_{CE}(f_j) + \mathcal{L}_{Tri}(f_j)) \quad (2)$$

\mathcal{L}_{base} benefits the ViT to elevate the discriminative power of both global and fine-grained part representations.

3.2 Prototypical Contrastive Learning.

The objective is to embed the positive pair nearby in the representation space while embedding negative pairs far apart. Note that each positive pair consists of an instance and its associated semantic prototype, while negative pairs consist of paired instances with unrelated semantic prototypes. Specifically, given a positive pair (v, c) , the ProtoNCE loss [21] is formulated below:

$$\mathcal{L}_{\text{ProtoNCE}}(v, c, \mathcal{N}_c, \{\tau_c\}) = -\log \frac{\exp(v \cdot c / \tau_c)}{\sum_{c_j \in \{c\} \cup \mathcal{N}_c} \exp(v \cdot c_j / \tau_{c_j})} \quad (3)$$

where \mathcal{N}_c denotes a set of negative prototypes for instance representation v , and τ_c is a prototype-specific temperature parameter.

4 METHOD

Fig. 2 shows the overall pipeline of Prototype-guided High-frequency Patch Enhancement (ProtoHPE), including ① Cross-modal High-freq Patch Enhancement (CHPE) and ② Multimodal Prototypical Contrast (MultiProCo). CHPE (Section 4.1) aims to enhance the representation ability of RGB-IR correlated high-freq patches. Then, both global and high-freq enhanced representations are regularized by MultiProCo (Section 4.2). MultiProCo hierarchically captures comprehensive semantics of different modal instances, facilitating the aggregation of representations belonging to the same identity.

4.1 Cross-modal High-freq Patch Enhancement

The objective is to enhance the representation ability of RGB-IR correlated high-freq patches that are more robust to the distribution shift than holistic images. Below, we explain the underlying mechanism of CHPE, which consists of (i) IR high-freq sampling and (ii) RGB-IR correlated high-freq patch enhancement.

(i) **IR high-freq sampling.** Given an IR person image $I \in \mathbb{R}^{H \times W \times C}$, where H , W and C represent its height, width and the number of channels respectively, we utilize Haar Wavelet Transform to decompose it into four wavelet subbands: I_{LL} , I_{LH} , I_{HL} , and $I_{HH} \in \mathbb{R}^{H/2 \times W/2 \times C}$. Note that I_{LL} mainly retains low-freq components that depict the overall appearance of a person image, while I_{LH} , I_{HL} , and I_{HH} reflect high-freq components that contain

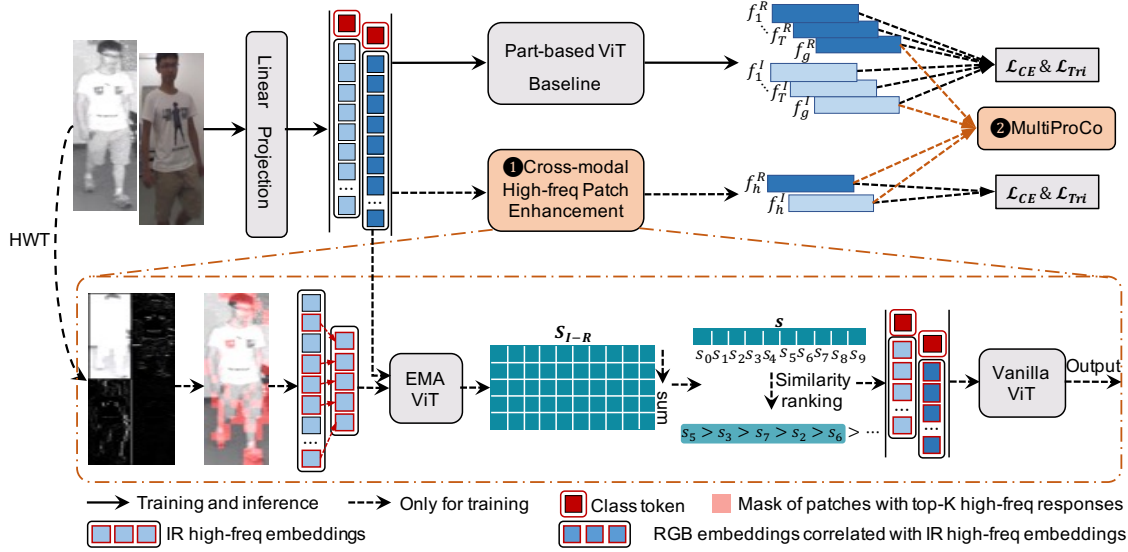


Figure 2: The overall of ProtoHPE, including ① Cross-modal High-freq Patch Enhancement (CHPE) and ② Multimodal Prototypical Contrast (MultiProCo). In CHPE, Haar Wavelet Transform (HWT) and an Exponential Moving Average ViT (EMA ViT) are jointly utilized to mine RGB-IR correlated high-freq patches. Such patches are then fed into vanilla ViT to enhance the representation ability of RGB-IR correlated high-freq components. Note that vanilla ViT and Part-based ViT share weights during training. MultiProCo hierarchically captures comprehensive semantics of different modal instances, facilitating the aggregation of global and high-freq enhanced representations belonging to the same identity. With it, The baseline can capture key high-freq components during inference without relying on ProtoHPE, thus bringing no extra complexity.

discriminative visual patterns such as heads and human silhouettes. Thus, we sum the later three subbands together:

$$M_h(I) = \text{sum}(I_{LH}, I_{HL}, I_{HH}), M_h(I) \in \mathbb{R}^{H/2 \times W/2 \times C} \quad (4)$$

We further introduce a projection function $\mathcal{G} : \mathbb{R}^{H/2 \times W/2 \times C} \rightarrow \mathbb{R}^{N \times C}$ to downsample $M_h(I)$ into N patches. Note that the projection \mathcal{G} is implemented by interpolation and flattening operations, without introducing additional trainable parameters. Then, we sample a subsequence of patches in Eq. (1), which contains patches with top- K high-freq responses:

$$\tilde{X}^I := \{\mathcal{F}(x_j^I) | x_j^I \in \text{top-}K(\|\mathcal{G}(M_h(I))\|_2)\} \quad (5)$$

where x_j^I denotes the j -th patch segmented from the IR modality image. \tilde{X}^I is the IR high-freq subsequence and $\|\cdot\|_2$ is the ℓ_2 -norm.

(ii) RGB-IR correlated high-freq patch enhancement. To capture RGB patches highly correlated with IR high-freq patches, an Exponential Moving Average ViT (EMA-ViT) $G(\theta'; \cdot)$ is introduced. Specifically, at each training iteration, we use $G(\theta'; \cdot)$ to encode both IR high-freq subsequence \tilde{X}^I and RGB entire sequence X^R :

$$\tilde{X}^I = G(\theta'; \tilde{X}^I), X^R = G(\theta'; X^R) \quad (6)$$

where the parameters θ' are updated from the Part-based ViT parameters θ : $\theta' = m\theta' + (1-m)\theta$, and m denotes the momentum factor close to 1, e.g., 0.9999. The parameters θ are updated by standard learning optimization. Given the encoded \tilde{X}^I and X^R in Eq. (6), we calculate the patch-level similarity matrix:

$$S_{I-R} = \tilde{X}^I X^{R^T}, S_{I-R} \in \mathbb{R}^{M \times N} \quad (7)$$

where M and N are the numbers of sampled IR high-freq patches and RGB whole patches, respectively. Each column vector of S_{I-R} indicates how similar each RGB embedding is to the IR high-freq patches. Thus, we run the row average of matrix S_{I-R} and generate a similarity vector $s \in \mathbb{R}^N$, in which the class token is excluded. Intuitively, a higher value in s implies that the corresponding RGB embedding is more correlated with IR high-freq patches. Hence, we directly select the RGB patches, which are with top- K values in s , as correlated visual patterns with \tilde{X}^I . Consequently, the selected RGB patches constitute the subsequence \tilde{X}^R :

$$\tilde{X}^R := \{\mathcal{F}(x_j^R) | s_j \in \text{top-}K(s)\} \quad (8)$$

where s_j is the j -th element of vector s . Afterward, the class token $x_{[\text{CLS}]}$ in Eq. (1) is prepended to the IR subsequence \tilde{X}^I in Eq. (5) and the RGB subsequence \tilde{X}^R in Eq. (8), respectively. Then we empower the vanilla ViT to take \tilde{X}^I and \tilde{X}^R as auxiliary input, and the encoded class tokens are served as the IR and RGB high-freq enhanced representations z^I and z^R , respectively. Note that vanilla ViT and Part-based ViT are weight-sharing during training. Subsequently, we optimize the representations z^I and z^R by minimizing the following objective:

$$\mathcal{L}_{\text{high}} = \mathcal{L}_{\text{CE}}(z^I) + \mathcal{L}_{\text{Tri}}(z^I) + \mathcal{L}_{\text{CE}}(z^R) + \mathcal{L}_{\text{Tri}}(z^R) \quad (9)$$

$\mathcal{L}_{\text{high}}$ benefits the ViT to enhance the representation ability and identity discrimination of RGB-IR correlated high-freq components, which are more robust to the distribution shift than holistic images.

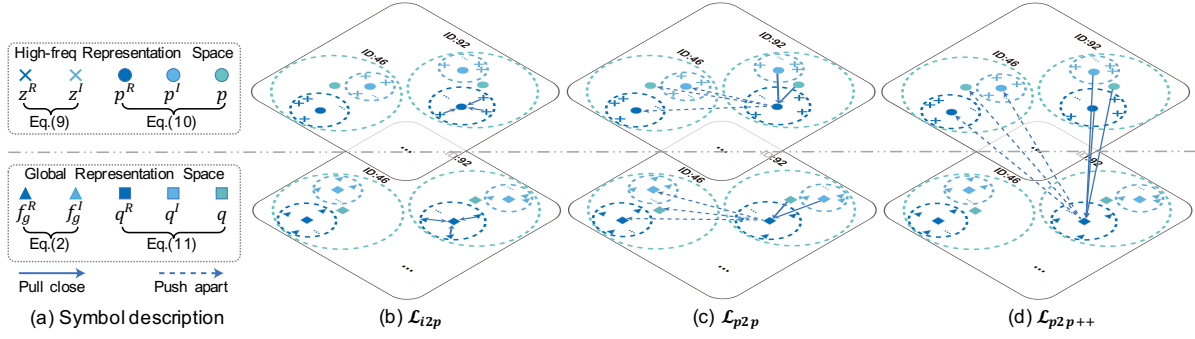


Figure 3: Illustration of MultiProCo. For notational simplicity, we only visualize the supervision on representations q^R and p^R of “ID:92”. \mathcal{L}_{i2p} synergizes with \mathcal{L}_{p2p} to hierarchically capture comprehensive semantics of different modal instances, thus facilitating the aggregation of representations belonging to the same identity. \mathcal{L}_{p2p++} benefits ViT to capture RGB-IR correlated high-freq components during inference without relying on ProtoHPE, thus bringing no extra complexity.

4.2 Multimodal Prototypical Contrast

In Eq. (9), \mathcal{L}_{high} optimizes representations z^R and z^I based only on instances in the mini-batch, ignoring comprehensive semantics of instances in different mini-batches. This may cause inconsistent representations of the same identity during network optimization.

To remedy such inadequacy, we propose Multimodal Prototypical Contrast (MultiProCo), as shown in Fig. 3. Note that a modality prototype is defined as a representative embedding for instances belonging to the same identity and the same modality. Below, we explain the underlying mechanism of MultiProCo, which consists of (i) **Multimodal Prototypes Construction and Update**, (ii) **Instance-Prototype Constraint**, and (iii) **Multimodal Prototypes Contrastive Regularization**.

(i) Multimodal Prototypes Construction and Update. To acquire stable multimodal prototypes, we directly construct and dynamically update the prototypes based on statistic centers of representations in each mini-batch. Given the enhanced RGB-IR correlated high-freq representations z^I and z^R , the multimodal high-freq prototypes of the c -th identity are formulated below:

$$p_c^I = \frac{1}{P} \sum_{y_i=c} z_i^I, p_c^R = \frac{1}{P} \sum_{y_i=c} z_i^R, p_c = \frac{1}{2P} \sum_{y_i=c} (z_i^I + z_i^R) \quad (10)$$

$$q_c^I = \frac{1}{P} \sum_{y_i=c} f_{g,i}^I, q_c^R = \frac{1}{P} \sum_{y_i=c} f_{g,i}^R, q_c = \frac{1}{2P} \sum_{y_i=c} (f_{g,i}^I + f_{g,i}^R) \quad (11)$$

where P is the number of IR/RGB instances per identity in a mini-batch, y_i is the identity label of the i -th instance, $f_{g,i}^I$ and $f_{g,i}^R$ denote the global representations of the i -th IR and RGB instances, respectively. Then, the above prototypes are dynamically updated by the exponential moving average. Taking the IR high-freq prototype as an example, we have:

$$p_c^I|_{\text{iter}} := \alpha p_c^I|_{\text{iter}} + (1 - \alpha) p_c^I|_{\text{iter}-1} \quad (12)$$

where α is the exponential decay rate and “iter” denotes the current training iteration.

(ii) Instance-Prototype Constraint. The purpose is to reduce intra-modal variations of instances belonging to the same identity. Specifically, we minimize the distance between feature representations and their corresponding modality prototypes. As shown

in Fig. 3 (b), the instance-prototype constraint is formulated below:

$$\mathcal{D}(a, b) = \|a - b\|_2 \quad (13)$$

$$\mathcal{L}_{i2p}^h = \frac{1}{P} \sum_{i=1}^P \mathcal{D}(z_i^I, p_{y_i}^I) + \frac{1}{P} \sum_{i=1}^P \mathcal{D}(z_i^R, p_{y_i}^R) + \frac{1}{2P} \sum_{i=1}^{2P} \mathcal{D}(z_i, p_{y_i}) \quad (14)$$

$$\mathcal{L}_{i2p}^g = \frac{1}{P} \sum_{i=1}^P \mathcal{D}(f_{g,i}^I, q_{y_i}^I) + \frac{1}{P} \sum_{i=1}^P \mathcal{D}(f_{g,i}^R, q_{y_i}^R) + \frac{1}{2P} \sum_{i=1}^{2P} \mathcal{D}(f_{g,i}, q_{y_i}) \quad (15)$$

$$\mathcal{L}_{i2p} = \mathcal{L}_{i2p}^g + \mathcal{L}_{i2p}^h \quad (16)$$

With \mathcal{L}_{i2p} , instances within a modality belonging to the same identity tend to aggregate together. However, \mathcal{L}_{i2p} neglects diverse semantics and structural distributions across different modalities and different identities. To this end, we further propose Multimodal Prototypes Contrastive Regularization below.

(iii) Multimodal Prototypes Contrastive Regularization. The objective is to create a representation space where multimodal prototypes belonging to the same identity are pulled together, while prototypes belonging to different identities are pushed apart.

In Fig. 3 (c), let $P_c = [p_c^I, p_c^R, p_c]$ and $Q_c = [q_c^I, q_c^R, q_c]$ denote the multimodal high-freq and global prototype sets of the c -th identity, respectively, we have:

$$S(a, b) = \exp\left(\frac{a \cdot b}{\|a\|_2 \cdot \|b\|_2} / \tau\right) \quad (17)$$

$$\mathcal{L}_{p2p}^h = \frac{1}{C} \sum_{c=1}^C \sum_{i=1}^C \log \frac{\sum_{j \neq i} S(P_{c,i}, P_{c,j})}{\sum_{j \neq i} S(P_{c,i}, P_{c,j}) + \sum_{k \neq c} \sum_{j=1}^C S(P_{c,i}, P_{k,j})} \quad (18)$$

$$\mathcal{L}_{p2p}^g = \frac{1}{C} \sum_{c=1}^C \sum_{i=1}^C \log \frac{\sum_{j \neq i} S(Q_{c,i}, Q_{c,j})}{\sum_{j \neq i} S(Q_{c,i}, Q_{c,j}) + \sum_{k \neq c} \sum_{j=1}^C S(Q_{c,i}, Q_{k,j})} \quad (19)$$

$$\mathcal{L}_{p2p} = \mathcal{L}_{p2p}^g + \mathcal{L}_{p2p}^h \quad (20)$$

where $P_{c,i}$ and $Q_{c,i}$ denote the i -th element of P_c and Q_c , respectively. τ is the temperature factor and C is the number of identities in the entire training set.

One distinct strength of MultiProCo over traditional instance contrast is that \mathcal{L}_{i2p} synergizes with \mathcal{L}_{p2p} to hierarchically capture comprehensive semantics of different modal instances. This

facilitates the aggregation of global and high-freq enhanced representations belonging to the same identity. With it, ViT can learn compact and informative representations to bridge the gap robustly.

To prevent RGB-IR correlated high-freq components from being suppressed by low-freq ones when taking the entire sequence Eq. (1) as input, we extend Eq. (20) to global and high-freq hybrid contrast:

$$\mathcal{L}_{p2p++} = \frac{1}{C} \sum_{c=1}^C \sum_{i=1}^C \log \frac{\sum_{j \neq i} S(\mathcal{Q}_{c,i}, \text{sg}(P_{c,j}))}{\sum_{j \neq i} S(\mathcal{Q}_{c,i}, \text{sg}(P_{c,j})) + \sum_{k \neq c} \sum_{j=1}^C S(\mathcal{Q}_{c,i}, \text{sg}(P_{k,j}))} \quad (21)$$

where “sg” denotes the stop-gradient operation. \mathcal{L}_{p2p++} benefits ViT to capture RGB-IR correlated high-freq components when taking the entire sequence Eq. (1) as input during inference. Hence, ProtoHPE is necessary during training and can be removed during inference, bringing no extra complexity. Finally, we optimize ProtoHPE by minimizing the overall objective:

$$\mathcal{L}_{overall} = \mathcal{L}_{base} + \mathcal{L}_{high} + \mathcal{L}_{i2p} + \mathcal{L}_{p2p} + \mathcal{L}_{p2p++} \quad (22)$$

5 EXPERIMENT

5.1 Dataset and Evaluation Protocol

SYSU-MM01 [36] is the first large-scale benchmark dataset for VI-ReID. Specifically, it contains 491 pedestrians with total 287,628 visible images and 15,792 infrared images, which are collected by 4 visible and 2 infrared cameras. Four cameras are deployed in the outdoor environments and two are deployed in the indoor environments. The training set contains 395 persons, including 22258 visible images and 11909 infrared images. The test set contains 96 persons, with 3,803 IR images for query and 301/3010 (one-shot/multi-shot) randomly selected RGB images as the gallery. Meanwhile, it contains two different testing settings, *all-search* and *indoor-search* settings, in which the *all-search* setting uses all images for testing and the *indoor-search* mode only uses the indoor images.

RegDB [36] is collected by a dual-camera system, including one visible and one infrared camera. It contains 412 identities, and each identity has 10 visible and 10 infrared images. Following previous evaluation protocol [34, 37], we randomly select all images of 206 identities for training and the remaining 206 identities for testing. The testing stage also contains two evaluation modes, *Visible-to-infrared* and *Infrared-to-visible* mode. The former means that the model retrieves the person in the infrared gallery when given a visible image, and vice versa. To obtain stable results, we randomly divide this dataset ten times for independent training and testing.

Following conventions [18, 19, 38], we adopt Cumulative Matching Characteristic (CMC) curves and the mean Average Precision (mAP) to evaluate the quality of different methods.

5.2 Implementation Details

All the experiments are performed on a single NVIDIA V100 GPU using the PyTorch framework. We adopt ViT-B/16 [11] as our backbone with initial weights pre-trained on ImageNet. We set the overlap stride to 12 to balance speed and performance and resize all person images to 256×128 . The training images are augmented with horizontal flipping and random erasing. For infrared images, color jitter and gaussian blur are additionally applied. The batch

size is set to 64 with a total of 8 different identities. For each identity, 4 visible images and 4 infrared images are sampled. We adopt AdamW optimizer with a cosine annealing learning rate scheduler for training. The basic learning rate is initialized as $3e^{-4}$ and weight decay is set to $1e^{-4}$. The parameter K in Eq. (5) is set to 30%. The exponential decay rate in Eq. (12) and the temperature factor in Eq. (17) are set to 0.8 and 0.1, respectively. The number of parts in the Part-based ViT baseline is set to 4.

5.3 Comparison with State-of-the-art Methods

Comparisons on SYSU-MM01. We compare ProtoHPE with the state-of-the-art approaches under both all-search and indoor-search settings in Table 1. Specifically, ProtoHPE achieves competitive performance, reaching 71.92%/70.59% and 77.81%/81.31% Rank-1/mAP in the all-search and indoor-search settings, respectively. From Table 1, we draw the following observations. (1) Compared with PMT [23] which is also based on the ViT framework, ProtoHPE outperforms it in both settings. The root reason is that PMT focuses on learning modality-shared features based on the correlation of RGB and IR holistic person images. This strategy may perform poorly under distribution shifts caused by large differences in wavelength, pose, and background clutter. In contrast, ProtoHPE effectively bridges the modality gap based on RGB-IR correlated high-freq components. Such components contain discriminative visual patterns and are more robust to the distribution shift than holistic images. (2) Compared to SMCL [34], which reduces the modality gap based only on instances in the mini-batch, one distinct strength of ProtoHPE is the ability to capture comprehensive semantics of different modalities. This facilitates the aggregation of representations belonging to the same identity, thereby learning compact and informative representations to robustly bridge the modality gap.

Comparisons on RegDB. In Table 2, ProtoHPE performs favorably against the state-of-the-art methods. Compared with DSC-Net [50], ProtoHPE outperforms it by 3.35%/6.42% Rank-1/mAP under the *Visible to Infrared* setting. For the more challenging *Infrared to Visible* setting, our ProtoHPE also achieves consistent improvement. Instead of aligning holistic person images, ProtoHPE bridges the modality gap based on RGB-IR correlated high-freq components, e.g., heads and human silhouettes, which are more robust to the distribution shift. The above results indicate that ProtoHPE performs robustly against different datasets and various query settings.

5.4 Ablation Study

We conduct ablation studies on SYSU-MM01 to analyze each core design, including Cross-modal High-freq Patch Enhancement (CHPE) and Multimodal Prototypical Contrast (MultiProCo). We consider the Part-based ViT as Baseline, and results are shown in Table 3.

Effectiveness of CHPE. From index-1 and index-2, CHPE greatly improves the Rank-1/mAP by 4.39%/6.45%. This indicates that enhancing RGB-IR correlated high-freq components is of great significance for boosting VI-ReID.

Effectiveness of \mathcal{L}_{i2p} in MultiProCo (Eq. (16)). From index-2 and index-3, \mathcal{L}_{i2p} improves the Rank-1/mAP by 1.08%/1.26%. The

Table 1: Comparison with the state-of-the-arts on SYSU-MM01 dataset. Rank-k accuracy and mAP are reported. Optimal and suboptimal results are highlighted in bold and underlined, respectively.

Settings		All-Search				Indoor-Search			
Method	Venue	R1 (%)	R10 (%)	R20 (%)	mAP (%)	R1 (%)	R10 (%)	R20 (%)	mAP (%)
cmGAN [10]	IJCAI18	26.97	67.51	80.56	27.80	31.63	77.23	89.18	42.19
AliGAN [31]	ICCV19	42.40	85.00	93.70	40.7	45.90	87.60	94.40	54.30
C MSP [35]	IJCV20	43.56	86.25	-	44.98	48.62	89.5	-	57.5
MACE [40]	TIP20	51.64	87.25	94.44	50.11	57.35	93.02	97.47	64.79
HCT [22]	TMM20	61.68	93.1	97.17	57.51	63.41	91.69	95.28	68.17
AGW [43]	TPAMI21	47.5	84.39	92.14	47.65	54.17	91.14	95.98	62.97
MCLNet [16]	ICCV21	65.40	93.3	97.14	61.98	<u>72.56</u>	96.88	99.20	<u>76.58</u>
SMCL [34]	ICCV21	67.39	92.87	96.76	61.78	68.84	96.55	98.77	75.56
CM-NAS [13]	CVPR21	61.99	92.87	97.25	60.02	67.01	<u>97.02</u>	<u>99.32</u>	72.95
MID [47]	AAAI22	60.27	-	-	59.40	64.86	-	-	70.12
SPOT [3]	TIP22	65.34	92.73	97.04	62.25	69.42	96.22	99.12	74.63
FMCNet [47]	CVPR22	66.74	-	-	62.51	68.15	-	-	74.09
PMT [23]	AAAI23	<u>67.53</u>	<u>95.36</u>	98.64	<u>64.98</u>	71.66	96.73	99.25	76.52
ProtoHPE	-	71.92	96.19	<u>97.98</u>	70.59	77.81	98.64	99.59	81.31

Table 2: Comparison with the state-of-the-arts on RegDB.

Settings		Visible to Infrared		Infrared to Visible	
Method	Venue	R1 (%)	mAP (%)	R1 (%)	mAP (%)
DG-VAE [28]	ACMMM20	72.97	71.78	-	-
HAT [44]	TIFS20	71.83	67.56	70.02	66.30
MACE [40]	TIP20	72.37	69.09	72.12	68.57
AGW [43]	TPAMI21	70.05	66.37	70.49	65.90
MCLNet [16]	ICCV21	80.31	73.07	75.93	69.49
CM-NAS [13]	ICCV21	84.54	80.32	82.57	78.31
CA [41]	ICCV21	85.03	79.14	<u>84.75</u>	77.82
NFS [8]	CVPR21	80.54	72.10	77.95	69.97
MPANet [37]	CVPR21	83.70	80.90	82.80	<u>80.70</u>
SPOT [3]	TIP22	80.35	72.46	79.37	72.26
MSCLNet [51]	ECCV22	84.17	<u>80.99</u>	83.86	78.31
PMT [23]	AAAI23	84.83	76.55	84.16	75.13
DSCNet [50]	TIFS23	<u>85.39</u>	77.30	83.50	75.19
ProtoHPE	-	88.74	83.72	88.69	81.99

Table 3: Ablation study over SYSU-MM01 dataset.

Index	Base	CHPE	MultiProCo			SYSU-MM01	
			\mathcal{L}_{i2p}	\mathcal{L}_{p2p}	\mathcal{L}_{p2p++}	R1 (%)	mAP (%)
1	✓					63.11	60.34
2	✓	✓				67.50	66.79
3	✓	✓	✓			68.58	68.05
4	✓	✓	✓	✓		69.73	68.92
5	✓	✓	✓	✓	✓	71.92	70.59

Table 4: Comparison in "MultiProCo vs Instance contrast" on SYSU-MM01.

Index	CHPE	Instance Contrast	MultiProCo	SYSU-MM01	
				R1 (%)	mAP (%)
1	✓	✓		69.18	66.94
2	✓		✓	71.92	70.59

improvement shows that \mathcal{L}_{i2p} benefits ViT to reduce the intra-modal variation of instances belonging to the same identity, thus extracting compact representations.

Effectiveness of \mathcal{L}_{p2p} in MultiProCo (Eq. (20)). From index-3 and index-4, \mathcal{L}_{p2p} elevates the Rank-1/mAP by 1.15%/0.87%. This indicates that \mathcal{L}_{p2p} synergizes with \mathcal{L}_{i2p} to hierarchically capture comprehensive semantics of different modal instances. This facilitates aggregating representations belonging to the same identity, thus robustly bridging the modality gap.

Effectiveness of \mathcal{L}_{p2p++} in MultiProCo (Eq. (21)). From index-4 and index-5, \mathcal{L}_{p2p++} improves the Rank-1/mAP by 2.19%/1.67%. The improvement indicates that \mathcal{L}_{p2p++} benefits the ViT to capture RGB-IR correlated high-freq components when taking the entire sequence Eq. (1) as input during inference. With it, ProtoHPE is necessary during training and can be removed during inference, without bringing extra complexity.

To further verify the effectiveness of MultiProCo, we conduct a comparison on "MultiProCo vs. Instance contrast". We implement it by replacing MultiProCo with traditional instance contrast, formulated as follows:

$$\mathcal{L}_{inst}^h = \frac{1}{B} \sum_{i=1}^B \log \frac{\sum_{j:y_j=y_i} \mathcal{S}(z_i^R, z_j^I)}{\sum_{j:y_j=y_i} \mathcal{S}(z_i^R, z_j^I) + \sum_{j:y_j \neq y_i} \mathcal{S}(z_i^R, z_j^I)} \quad (23)$$

$$\mathcal{L}_{inst}^g = \frac{1}{B} \sum_{i=1}^B \log \frac{\sum_{j:y_j=y_i} \mathcal{S}(f_{g,i}^R, f_{g,j}^I)}{\sum_{j:y_j=y_i} \mathcal{S}(f_{g,i}^R, f_{g,j}^I) + \sum_{j:y_j \neq y_i} \mathcal{S}(f_{g,i}^R, f_{g,j}^I)} \quad (24)$$

$$\mathcal{L}_{inst} = \mathcal{L}_{inst}^g + \mathcal{L}_{inst}^h \quad (25)$$

where B is the number of IR/RGB instances in a mini-batch. The result in Table 4 shows that compared to \mathcal{L}_{inst} that bridges the modality gap based only on instances in the mini-batch, MultiProCo facilitates extracting more compact and more discriminative representations to bridge the modality gap robustly.

Analysis on the distribution of positive and negative pairs.

Fig. 5 shows the Euclidean distance distribution of positive and negative pairs on SYSU-MM01 during inference. Compared to Baseline, ProtoHPE reduces the mean distance of positive pairs from 1.37 to 1.18, while increasing the mean distance between positive and negative distributions from 0.57 to 0.74. The above result shows that ProtoHPE benefits Baseline to effectively reduce the modality

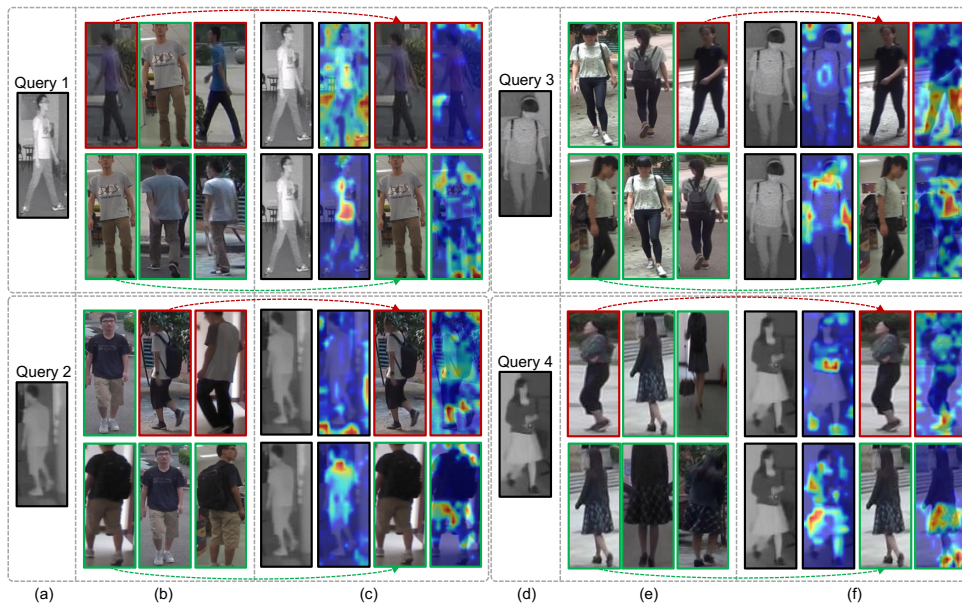


Figure 4: Comparisons in top-3 retrieval results and attention maps between Baseline and ProtoHPE on SYSU-MM01. Given each IR query in (a) and (d), the 1st and 2nd rows in (b) and (e) show the top-3 retrieval results of Baseline and ProtoHPE, respectively. There are errors in the retrieval results of Baseline (highlighted in red boxes), while the results of ProtoHPE are all correct (highlighted in green boxes). In (c) and (f), we visualize the attention maps of Baseline on the query and wrong retrieval result (the 1st row), and the attention maps of ProtoHPE on the query and correct retrieval result (the 2nd row).

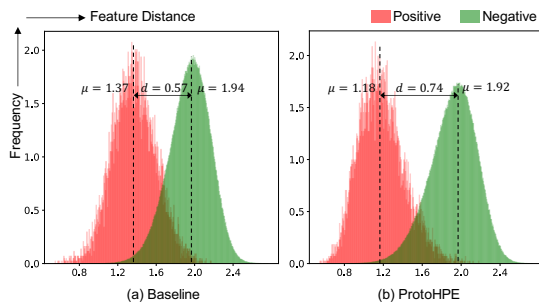


Figure 5: Euclidean distance distribution of positive and negative pairs on SYSU-MM01 during inference.

gap of instances belonging to the same identity, while pushing instances belonging to different identities away from each other.

5.5 Visualization Analysis

Fig. 4 shows comparisons in top-3 retrieval results and attention maps between Baseline and ProtoHPE on SYSU-MM01 during inference. Taking the IR query “Query 1” in Fig. 4 (a) as an example, the 1st and 2nd rows in Fig. 4 (b) show the top-3 retrieval results of Baseline and ProtoHPE, respectively. Compared to Baseline which incorrectly matches person images with different identities from the query (highlighted in red boxes), ProtoHPE can correctly identify person images with the same identity as the query (highlighted in green boxes). To further explain the effectiveness of ProtoHPE

against Baseline, we utilize Grad-CAM to visualize the attention maps of Baseline on “Query 1” and the wrong retrieval result (the 1st row in Fig. 4 (c)), and the attention maps of ProtoHPE on “Query 1” and the correct retrieval result (the 2nd row in Fig. 4 (c)). We can see that Baseline mistakenly takes the background clutter as discriminative parts, thereby leading to wrong retrieval results. In contrast, our ProtoHPE yields lower responses on the background and low-freq components, while focusing on RGB-IR correlated high-freq components, such as heads and human silhouettes.

6 CONCLUSION

In this work, we developed Prototype-guided High-frequency Patch Enhancement, termed ProtoHPE, for visible-infrared person re-identification. We propose Cross-modal High-freq Patch Enhancement, which enhances the representation ability of RGB-IR correlated high-freq components. Such components contain discriminative visual patterns that are less affected by the distribution shift than holistic images. To extract semantically compact and informative representations of the same identity, we propose Multimodal Prototypical Contrast (MultiProCo). MultiProCo hierarchically captures comprehensive semantics of different modal instances, facilitating the aggregation of representations belonging to the same identity. Extensive experimental results perform favorably against mainstream methods on SYSU-MM01 and RegDB datasets. **Acknowledgements.** This work was partially supported by the National Natural Science Foundation of China (No. 62072022) and the Fundamental Research Funds for the Central Universities.

REFERENCES

- [1] Alex Andonian, Shixing Chen, and Raffay Hamid. 2022. Robust cross-modal representation learning with progressive self-distillation. In *Proceedings of the IEEE/CVF Conference on Computer Vision and Pattern Recognition*. 16430–16441.
- [2] Mathilde Caron, Hugo Touvron, Ishan Misra, Hervé Jégou, Julien Mairal, Piotr Bojanowski, and Armand Joulin. 2021. Emerging properties in self-supervised vision transformers. In *Proceedings of the IEEE/CVF international conference on computer vision*. 9650–9660.
- [3] Cuiqun Chen, Mang Ye, Meibin Qi, Jingjing Wu, Jianguo Jiang, and Chia-Wen Lin. 2022. Structure-aware positional transformer for visible-infrared person re-identification. *IEEE Transactions on Image Processing* 31 (2022), 2352–2364.
- [4] Delong Chen, Zhao Wu, Fan Liu, Zaiquan Yang, Yixiang Huang, Yiping Bao, and Erjin Zhou. 2022. Prototypical Contrastive Language Image Pretraining. *arXiv preprint arXiv:2206.10996* (2022).
- [5] Ting Chen, Simon Kornblith, Mohammad Norouzi, and Geoffrey Hinton. 2020. A simple framework for contrastive learning of visual representations. In *International conference on machine learning*. PMLR, 1597–1607.
- [6] Xinlei Chen and Kaiming He. 2021. Exploring simple siamese representation learning. In *Proceedings of the IEEE/CVF conference on computer vision and pattern recognition*. 15750–15758.
- [7] Xinlei Chen, Saining Xie, and Kaiming He. 2021. An empirical study of training self-supervised vision transformers. In *Proceedings of the IEEE/CVF International Conference on Computer Vision*. 9640–9649.
- [8] Yehansen Chen, Lin Wan, Zhihang Li, Qianyan Jing, and Zongyuan Sun. 2021. Neural feature search for rgb-infrared person re-identification. In *Proceedings of the IEEE/CVF Conference on Computer Vision and Pattern Recognition*. 587–597.
- [9] Seokeon Choi, Sumin Lee, Youngeun Kim, Taekyung Kim, and Changick Kim. 2020. Hi-CMD: Hierarchical cross-modality disentanglement for visible-infrared person re-identification. In *Proceedings of the IEEE/CVF conference on computer vision and pattern recognition*. 10257–10266.
- [10] Pingyang Dai, Rongrong Ji, Haibin Wang, Qiong Wu, and Yuyu Huang. 2018. Cross-modality person re-identification with generative adversarial training. In *IJCAI*, Vol. 1. 6.
- [11] Alexey Dosovitskiy, Lucas Beyer, Alexander Kolesnikov, Dirk Weissenborn, Xi-aohua Zhai, Thomas Unterthiner, Mostafa Dehghani, Matthias Minderer, Georg Heigold, Sylvain Gelly, et al. 2020. An image is worth 16x16 words: Transformers for image recognition at scale. *arXiv preprint arXiv:2010.11929* (2020).
- [12] Linus Ericsson, Henry Gouk, Chen Change Loy, and Timothy M Hospedales. 2022. Self-supervised representation learning: Introduction, advances, and challenges. *IEEE Signal Processing Magazine* 39, 3 (2022), 42–62.
- [13] Chaoyou Fu, Yibo Hu, Xiang Wu, Hailin Shi, Tao Mei, and Ran He. 2021. CM-NAS: Cross-modality neural architecture search for visible-infrared person re-identification. In *Proceedings of the IEEE/CVF International Conference on Computer Vision*. 11823–11832.
- [14] Shin Fujieda, Kohei Takayama, and Toshiya Hachisuka. 2018. Wavelet convolutional neural networks. *arXiv preprint arXiv:1805.08620* (2018).
- [15] Yajun Gao, Tengfei Liang, Yi Jin, Xiaoyan Gu, Wu Liu, Yidong Li, and Congyan Lang. 2021. MSO: Multi-feature space joint optimization network for rgb-infrared person re-identification. In *Proceedings of the 29th ACM International Conference on Multimedia*. 5257–5265.
- [16] Xin Hao, Sanyuan Zhao, Mang Ye, and Jianbing Shen. 2021. Cross-modality person re-identification via modality confusion and center aggregation. In *Proceedings of the IEEE/CVF International Conference on Computer Vision*. 16403–16412.
- [17] Kaiming He, Haoqi Fan, Yuxin Wu, Saining Xie, and Ross Girshick. 2020. Momentum contrast for unsupervised visual representation learning. In *Proceedings of the IEEE/CVF conference on computer vision and pattern recognition*. 9729–9738.
- [18] Lingxiao He, Xingyu Liao, Wu Liu, Xinchun Liu, Peng Cheng, and Tao Mei. 2020. Fastreid: A pytorch toolbox for general instance re-identification. *arXiv preprint arXiv:2006.02631* (2020).
- [19] Shuting He, Hao Luo, Pichao Wang, Fan Wang, Hao Li, and Wei Jiang. 2021. Transreid: Transformer-based object re-identification. In *Proceedings of the IEEE/CVF International Conference on Computer Vision*. 15013–15022.
- [20] Kongzhu Jiang, Tianzhu Zhang, Xiang Liu, Bingqiao Qian, Yongdong Zhang, and Feng Wu. 2022. Cross-Modality Transformer for Visible-Infrared Person Re-Identification. In *European Conference on Computer Vision*. Springer, 480–496.
- [21] Junnan Li, Pan Zhou, Caiming Xiong, and Steven CH Hoi. 2020. Prototypical contrastive learning of unsupervised representations. *arXiv preprint arXiv:2005.04966* (2020).
- [22] Haijun Liu, Xiaoheng Tan, and Xichuan Zhou. 2020. Parameter sharing exploration and hetero-center triplet loss for visible-thermal person re-identification. *IEEE Transactions on Multimedia* 23 (2020), 4414–4425.
- [23] Hu Lu, Xuezhang Zou, and Pingping Zhang. 2022. Learning Progressive Modality-shared Transformers for Effective Visible-Infrared Person Re-identification. *arXiv preprint arXiv:2212.00226* (2022).
- [24] Yan Lu, Yue Wu, Bin Liu, Tianzhu Zhang, Baopu Li, Qi Chu, and Nenghai Yu. 2020. Cross-modality person re-identification with shared-specific feature transfer. In *Proceedings of the IEEE/CVF Conference on Computer Vision and Pattern Recognition*. 13379–13389.
- [25] Yiwei Ma, Guohai Xu, Xiaoshuai Sun, Ming Yan, Ji Zhang, and Rongrong Ji. 2022. X-CLIP: End-to-End Multi-grained Contrastive Learning for Video-Text Retrieval. In *Proceedings of the 30th ACM International Conference on Multimedia*. 638–647.
- [26] Changtao Miao, Zichang Tan, Qi Chu, Huan Liu, Honggang Hu, and Nenghai Yu. 2023. F 2 Trans: High-Frequency Fine-Grained Transformer for Face Forgery Detection. *IEEE Transactions on Information Forensics and Security* 18 (2023), 1039–1051.
- [27] Changtao Miao, Zichang Tan, Qi Chu, Nenghai Yu, and Guodong Guo. 2022. Hierarchical frequency-assisted interactive networks for face manipulation detection. *IEEE Transactions on Information Forensics and Security* 17 (2022), 3008–3021.
- [28] Nan Pu, Wei Chen, Yu Liu, Erwin M Bakker, and Michael S Lew. 2020. Dual gaussian-based variational subspace disentanglement for visible-infrared person re-identification. In *Proceedings of the 28th ACM International Conference on Multimedia*. 2149–2158.
- [29] Alec Radford, Jong Wook Kim, Chris Hallacy, Aditya Ramesh, Gabriel Goh, Sandhini Agarwal, Girish Sastry, Amanda Askell, Pamela Mishkin, Jack Clark, et al. 2021. Learning transferable visual models from natural language supervision. In *International conference on machine learning*. PMLR, 8748–8763.
- [30] Lei Tan, Pingyang Dai, Rongrong Ji, and Yongjian Wu. 2022. Dynamic Prototype Mask for Occluded Person Re-Identification. In *Proceedings of the 30th ACM International Conference on Multimedia*. 531–540.
- [31] Guan'an Wang, Tianzhu Zhang, Jian Cheng, Si Liu, Yang Yang, and Zengguang Hou. 2019. RGB-infrared cross-modality person re-identification via joint pixel and feature alignment. In *Proceedings of the IEEE/CVF International Conference on Computer Vision*. 3623–3632.
- [32] Guan-An Wang, Tianzhu Zhang, Yang Yang, Jian Cheng, Jianlong Chang, Xu Liang, and Zeng-Guang Hou. 2020. Cross-modality paired-images generation for RGB-infrared person re-identification. In *Proceedings of the AAAI conference on artificial intelligence*, Vol. 34. 12144–12151.
- [33] Zhixiang Wang, Zheng Wang, Yingqiang Zheng, Yung-Yu Chuang, and Shin'ichi Satoh. 2019. Learning to reduce dual-level discrepancy for infrared-visible person re-identification. In *Proceedings of the IEEE/CVF Conference on Computer Vision and Pattern Recognition*. 618–626.
- [34] Ziyu Wei, Xi Yang, Nannan Wang, and Xinbo Gao. 2021. Syncretic modality collaborative learning for visible infrared person re-identification. In *Proceedings of the IEEE/CVF International Conference on Computer Vision*. 225–234.
- [35] Ancong Wu, Wei-Shi Zheng, Shaogang Gong, and Jianhuang Lai. 2020. Rgb-ir person re-identification by cross-modality similarity preservation. *International journal of computer vision* 128, 6 (2020), 1765–1785.
- [36] Ancong Wu, Wei-Shi Zheng, Hong-Xing Yu, Shaogang Gong, and Jianhuang Lai. 2017. RGB-infrared cross-modality person re-identification. In *Proceedings of the IEEE international conference on computer vision*. 5380–5389.
- [37] Qiong Wu, Pingyang Dai, Jie Chen, Chia-Wen Lin, Yongjian Wu, Feiyue Huang, Bineng Zhong, and Rongrong Ji. 2021. Discover cross-modality nuances for visible-infrared person re-identification. In *Proceedings of the IEEE/CVF Conference on Computer Vision and Pattern Recognition*. 4330–4339.
- [38] Cheng Yan, Guansong Pang, Xiao Bai, Changhong Liu, Ning Xin, Lin Gu, and Jun Zhou. 2021. Beyond triplet loss: person re-identification with fine-grained difference-aware pairwise loss. *IEEE Transactions on Multimedia* (2021).
- [39] Ting Yao, Yingwei Pan, Yehao Li, Chong-Wah Ngo, and Tao Mei. 2022. Wave-vit: Unifying wavelet and transformers for visual representation learning. *arXiv preprint arXiv:2207.04978* (2022).
- [40] Mang Ye, Xiangyuan Lan, Qingming Leng, and Jianbing Shen. 2020. Cross-modality person re-identification via modality-aware collaborative ensemble learning. *IEEE Transactions on Image Processing* 29 (2020), 9387–9399.
- [41] Mang Ye, Weijian Ruan, Bo Du, and Mike Zheng Shou. 2021. Channel augmented joint learning for visible-infrared recognition. In *Proceedings of the IEEE/CVF International Conference on Computer Vision*. 13567–13576.
- [42] Mang Ye, Jianbing Shen, David J Crandall, Ling Shao, and Jiebo Luo. 2020. Dynamic dual-attentive aggregation learning for visible-infrared person re-identification. In *European Conference on Computer Vision*. Springer, 229–247.
- [43] Mang Ye, Jianbing Shen, Gaojie Lin, Tao Xiang, Ling Shao, and Steven CH Hoi. 2021. Deep learning for person re-identification: A survey and outlook. *IEEE transactions on pattern analysis and machine intelligence* 44, 6 (2021), 2872–2893.
- [44] Mang Ye, Jianbing Shen, and Ling Shao. 2020. Visible-infrared person re-identification via homogeneous augmented tri-modal learning. *IEEE Transactions on Information Forensics and Security* 16 (2020), 728–739.
- [45] Guiwei Zhang, Yongfei Zhang, Tianyu Zhang, Bo Li, and Shiliang Pu. 2023. PHA: Patch-Wise High-Frequency Augmentation for Transformer-Based Person Re-Identification. In *Proceedings of the IEEE/CVF Conference on Computer Vision and Pattern Recognition*. 14133–14142.
- [46] Liyan Zhang, Guodong Du, Fan Liu, Huawei Tu, and Xiangbo Shu. 2021. Global-local multiple granularity learning for cross-modality visible-infrared person reidentification. *IEEE Transactions on Neural Networks and Learning Systems* (2021).
- [47] Qiang Zhang, Changzhou Lai, Jianan Liu, Nianchang Huang, and Jungong Han. 2022. Fmcnet: Feature-level modality compensation for visible-infrared person

re-identification. In *Proceedings of the IEEE/CVF Conference on Computer Vision and Pattern Recognition*. 7349–7358.

- [48] Tianyu Zhang, Lingxi Xie, Longhui Wei, Yongfei Zhang, Bo Li, and Qi Tian. 2020. Single camera training for person re-identification. In *Proceedings of the AAAI Conference on Artificial Intelligence*, Vol. 34. 12878–12885.
- [49] Tianyu Zhang, Lingxi Xie, Longhui Wei, Zijie Zhuang, Yongfei Zhang, Bo Li, and Qi Tian. 2021. Unreal person: An adaptive pipeline towards costless person re-identification. In *Proceedings of the IEEE/CVF Conference on Computer Vision and Pattern Recognition*. 11506–11515.
- [50] Yiyuan Zhang, Yuhao Kang, Sanyuan Zhao, and Jianbing Shen. 2022. Dual-Semantic Consistency Learning for Visible-Infrared Person Re-Identification. *IEEE Transactions on Information Forensics and Security* 18 (2022), 1554–1565.
- [51] Yiyuan Zhang, Sanyuan Zhao, Yuhao Kang, and Jianbing Shen. 2022. Modality Synergy Complement Learning with Cascaded Aggregation for Visible-Infrared Person Re-Identification. In *European Conference on Computer Vision*. Springer, 462–479.
- [52] Kuan Zhu, Haiyun Guo, Tianyi Yan, Yousong Zhu, Jinqiao Wang, and Ming Tang. 2022. Part-Aware Self-Supervised Pre-Training for Person Re-Identification. *arXiv preprint arXiv:2203.03931* (2022).
- ## REFERENCES
- [1] Alex Andonian, Shixing Chen, and Raffay Hamid. 2022. Robust cross-modal representation learning with progressive self-distillation. In *Proceedings of the IEEE/CVF Conference on Computer Vision and Pattern Recognition*. 16430–16441.
- [2] Mathilde Caron, Hugo Touvron, Ishan Misra, Hervé Jégou, Julien Mairal, Piotr Bojanowski, and Armand Joulin. 2021. Emerging properties in self-supervised vision transformers. In *Proceedings of the IEEE/CVF international conference on computer vision*. 9650–9660.
- [3] Cuiqun Chen, Mang Ye, Meibin Qi, Jingjing Wu, Jianguo Jiang, and Chia-Wen Lin. 2022. Structure-aware positional transformer for visible-infrared person re-identification. *IEEE Transactions on Image Processing* 31 (2022), 2352–2364.
- [4] Delong Chen, Zhao Wu, Fan Liu, Zaiquan Yang, Yixiang Huang, Yiping Bao, and Erjin Zhou. 2022. Prototypical Contrastive Language Image Pretraining. *arXiv preprint arXiv:2206.10996* (2022).
- [5] Ting Chen, Simon Kornblith, Mohammad Norouzi, and Geoffrey Hinton. 2020. A simple framework for contrastive learning of visual representations. In *International conference on machine learning*. PMLR, 1597–1607.
- [6] Xinlei Chen and Kaiming He. 2021. Exploring simple siamese representation learning. In *Proceedings of the IEEE/CVF conference on computer vision and pattern recognition*. 15750–15758.
- [7] Xinlei Chen, Saining Xie, and Kaiming He. 2021. An empirical study of training self-supervised vision transformers. In *Proceedings of the IEEE/CVF International Conference on Computer Vision*. 9640–9649.
- [8] Yehansen Chen, Lin Wan, Zhihang Li, Qianyan Jing, and Zongyuan Sun. 2021. Neural feature search for rgb-infrared person re-identification. In *Proceedings of the IEEE/CVF Conference on Computer Vision and Pattern Recognition*. 587–597.
- [9] Seokeon Choi, Sumin Lee, Youngeun Kim, Taekyung Kim, and Changick Kim. 2020. Hi-CMD: Hierarchical cross-modality disentanglement for visible-infrared person re-identification. In *Proceedings of the IEEE/CVF conference on computer vision and pattern recognition*. 10257–10266.
- [10] Pingyang Dai, Rongrong Ji, Haibin Wang, Qiong Wu, and Yuyu Huang. 2018. Cross-modality person re-identification with generative adversarial training. In *IJCAI*, Vol. 1. 6.
- [11] Alexey Dosovitskiy, Lucas Beyer, Alexander Kolesnikov, Dirk Weissenborn, Xiuhua Zhai, Thomas Unterthiner, Mostafa Dehghani, Matthias Minderer, Georg Heigold, Sylvain Gelly, et al. 2020. An image is worth 16x16 words: Transformers for image recognition at scale. *arXiv preprint arXiv:2010.11929* (2020).
- [12] Linus Ericsson, Henry Gouk, Chen Change Loy, and Timothy M Hospedales. 2022. Self-supervised representation learning: Introduction, advances, and challenges. *IEEE Signal Processing Magazine* 39, 3 (2022), 42–62.
- [13] Chaoyou Fu, Yibo Hu, Xiang Wu, Hailin Shi, Tao Mei, and Ran He. 2021. CM-NAS: Cross-modality neural architecture search for visible-infrared person re-identification. In *Proceedings of the IEEE/CVF International Conference on Computer Vision*. 11823–11832.
- [14] Shin Fujieda, Kohei Takayama, and Toshiya Hachisuka. 2018. Wavelet convolutional neural networks. *arXiv preprint arXiv:1805.08620* (2018).
- [15] Yajun Gao, Tengfei Liang, Yi Jin, Xiaoyan Gu, Wu Liu, Yidong Li, and Congyan Lang. 2021. MSO: Multi-feature space joint optimization network for rgb-infrared person re-identification. In *Proceedings of the 29th ACM International Conference on Multimedia*. 5257–5265.
- [16] Xin Hao, Sanyuan Zhao, Mang Ye, and Jianbing Shen. 2021. Cross-modality person re-identification via modality confusion and center aggregation. In *Proceedings of the IEEE/CVF International Conference on Computer Vision*. 16403–16412.
- [17] Kaiming He, Haoqi Fan, Yuxin Wu, Saining Xie, and Ross Girshick. 2020. Momentum contrast for unsupervised visual representation learning. In *Proceedings of the IEEE/CVF conference on computer vision and pattern recognition*. 9729–9738.
- [18] Lingxiao He, Xingyu Liao, Wu Liu, Xinchun Liu, Peng Cheng, and Tao Mei. 2020. Fastreid: A pytorch toolbox for general instance re-identification. *arXiv preprint arXiv:2006.02631* (2020).
- [19] Shuting He, Hao Luo, Pichao Wang, Fan Wang, Hao Li, and Wei Jiang. 2021. Transreid: Transformer-based object re-identification. In *Proceedings of the IEEE/CVF International Conference on Computer Vision*. 15013–15022.
- [20] Kongzhu Jiang, Tianzhu Zhang, Xiang Liu, Bingqiao Qian, Yongdong Zhang, and Feng Wu. 2022. Cross-Modality Transformer for Visible-Infrared Person Re-Identification. In *European Conference on Computer Vision*. Springer, 480–496.
- [21] Junnan Li, Pan Zhou, Caiming Xiong, and Steven CH Hoi. 2020. Prototypical contrastive learning of unsupervised representations. *arXiv preprint arXiv:2005.04966* (2020).
- [22] Haijun Liu, Xiaoheng Tan, and Xichuan Zhou. 2020. Parameter sharing exploration and hetero-center triplet loss for visible-thermal person re-identification. *IEEE Transactions on Multimedia* 23 (2020), 4414–4425.
- [23] Hu Lu, Xuezhong Zou, and Pingping Zhang. 2022. Learning Progressive Modality-shared Transformers for Effective Visible-Infrared Person Re-identification. *arXiv preprint arXiv:2212.00226* (2022).
- [24] Yan Lu, Yue Wu, Bin Liu, Tianzhu Zhang, Baopu Li, Qi Chu, and Nenghai Yu. 2020. Cross-modality person re-identification with shared-specific feature transfer. In *Proceedings of the IEEE/CVF Conference on Computer Vision and Pattern Recognition*. 13379–13389.
- [25] Yiwei Ma, Guohai Xu, Xiaoshuai Sun, Ming Yan, Ji Zhang, and Rongrong Ji. 2022. X-CLIP: End-to-End Multi-grained Contrastive Learning for Video-Text Retrieval. In *Proceedings of the 30th ACM International Conference on Multimedia*. 638–647.
- [26] Changtao Miao, Zichang Tan, Qi Chu, Huan Liu, Honggang Hu, and Nenghai Yu. 2023. F 2 Trans: High-Frequency Fine-Grained Transformer for Face Forgery Detection. *IEEE Transactions on Information Forensics and Security* 18 (2023), 1039–1051.
- [27] Changtao Miao, Zichang Tan, Qi Chu, Nenghai Yu, and Guodong Guo. 2022. Hierarchical frequency-assisted interactive networks for face manipulation detection. *IEEE Transactions on Information Forensics and Security* 17 (2022), 3008–3021.
- [28] Nan Pu, Wei Chen, Yu Liu, Erwin M Bakker, and Michael S Lew. 2020. Dual gaussian-based variational subspace disentanglement for visible-infrared person re-identification. In *Proceedings of the 28th ACM International Conference on Multimedia*. 2149–2158.
- [29] Alec Radford, Jong Wook Kim, Chris Hallacy, Aditya Ramesh, Gabriel Goh, Sandhini Agarwal, Girish Sastry, Amanda Askell, Pamela Mishkin, Jack Clark, et al. 2021. Learning transferable visual models from natural language supervision. In *International conference on machine learning*. PMLR, 8748–8763.
- [30] Lei Tan, Pingyang Dai, Rongrong Ji, and Yongjian Wu. 2022. Dynamic Prototype Mask for Occluded Person Re-Identification. In *Proceedings of the 30th ACM International Conference on Multimedia*. 531–540.
- [31] Guan'an Wang, Tianzhu Zhang, Jian Cheng, Si Liu, Yang Yang, and Zengguang Hou. 2019. RGB-infrared cross-modality person re-identification via joint pixel and feature alignment. In *Proceedings of the IEEE/CVF International Conference on Computer Vision*. 3623–3632.
- [32] Guan-An Wang, Tianzhu Zhang, Yang Yang, Jian Cheng, Jianlong Chang, Xu Liang, and Zeng-Guang Hou. 2020. Cross-modality paired-images generation for RGB-infrared person re-identification. In *Proceedings of the AAAI conference on artificial intelligence*, Vol. 34. 12144–12151.
- [33] Zhixiang Wang, Zheng Wang, Yinqiang Zheng, Yung-Yu Chuang, and Shin'ichi Satoh. 2019. Learning to reduce dual-level discrepancy for infrared-visible person re-identification. In *Proceedings of the IEEE/CVF Conference on Computer Vision and Pattern Recognition*. 618–626.
- [34] Ziyu Wei, Xi Yang, Nannan Wang, and Xinbo Gao. 2021. Synergetic modality collaborative learning for visible infrared person re-identification. In *Proceedings of the IEEE/CVF International Conference on Computer Vision*. 225–234.
- [35] Ancong Wu, Wei-Shi Zheng, Shaogang Gong, and Jianhuang Lai. 2020. Rgb-ir person re-identification by cross-modality similarity preservation. *International journal of computer vision* 128, 6 (2020), 1765–1785.
- [36] Ancong Wu, Wei-Shi Zheng, Hong-Xing Yu, Shaogang Gong, and Jianhuang Lai. 2017. RGB-infrared cross-modality person re-identification. In *Proceedings of the IEEE international conference on computer vision*. 5380–5389.
- [37] Qiong Wu, Pingyang Dai, Jie Chen, Chia-Wen Lin, Yongjian Wu, Feiyue Huang, Bineng Zhong, and Rongrong Ji. 2021. Discover cross-modality nuances for visible-infrared person re-identification. In *Proceedings of the IEEE/CVF Conference on Computer Vision and Pattern Recognition*. 4330–4339.
- [38] Cheng Yan, Guansong Pang, Xiao Bai, Changhong Liu, Ning Xin, Lin Gu, and Jun Zhou. 2021. Beyond triplet loss: person re-identification with fine-grained difference-aware pairwise loss. *IEEE Transactions on Multimedia* (2021).
- [39] Ting Yao, Yingwei Pan, Yehao Li, Chong-Wah Ngo, and Tao Mei. 2022. Wave-vit: Unifying wavelet and transformers for visual representation learning. *arXiv preprint arXiv:2207.04978* (2022).
- [40] Mang Ye, Xiangyuan Lan, Qingming Leng, and Jianbing Shen. 2020. Cross-modality person re-identification via modality-aware collaborative ensemble learning. *IEEE Transactions on Image Processing* 29 (2020), 9387–9399.
- [41] Mang Ye, Weijian Ruan, Bo Du, and Mike Zheng Shou. 2021. Channel augmented joint learning for visible-infrared recognition. In *Proceedings of the IEEE/CVF*

International Conference on Computer Vision. 13567–13576.

[42] Mang Ye, Jianbing Shen, David J Crandall, Ling Shao, and Jiebo Luo. 2020. Dynamic dual-attentive aggregation learning for visible-infrared person re-identification. In *European Conference on Computer Vision*. Springer, 229–247.

[43] Mang Ye, Jianbing Shen, Gaojie Lin, Tao Xiang, Ling Shao, and Steven CH Hoi. 2021. Deep learning for person re-identification: A survey and outlook. *IEEE transactions on pattern analysis and machine intelligence* 44, 6 (2021), 2872–2893.

[44] Mang Ye, Jianbing Shen, and Ling Shao. 2020. Visible-infrared person re-identification via homogeneous augmented tri-modal learning. *IEEE Transactions on Information Forensics and Security* 16 (2020), 728–739.

[45] Guiwei Zhang, Yongfei Zhang, Tianyu Zhang, Bo Li, and Shiliang Pu. 2023. PHA: Patch-Wise High-Frequency Augmentation for Transformer-Based Person Re-Identification. In *Proceedings of the IEEE/CVF Conference on Computer Vision and Pattern Recognition*. 14133–14142.

[46] Liyan Zhang, Guodong Du, Fan Liu, Huawei Tu, and Xiangbo Shu. 2021. Global-local multiple granularity learning for cross-modality visible-infrared person reidentification. *IEEE Transactions on Neural Networks and Learning Systems* (2021).

[47] Qiang Zhang, Changzhou Lai, Jianan Liu, Nianchang Huang, and Jungong Han. 2022. Fmcnet: Feature-level modality compensation for visible-infrared person re-identification. In *Proceedings of the IEEE/CVF Conference on Computer Vision and Pattern Recognition*. 7349–7358.

[48] Tianyu Zhang, Lingxi Xie, Longhui Wei, Yongfei Zhang, Bo Li, and Qi Tian. 2020. Single camera training for person re-identification. In *Proceedings of the AAAI Conference on Artificial Intelligence*, Vol. 34. 12878–12885.

[49] Tianyu Zhang, Lingxi Xie, Longhui Wei, Zijie Zhuang, Yongfei Zhang, Bo Li, and Qi Tian. 2021. Unrealperson: An adaptive pipeline towards costless person re-identification. In *Proceedings of the IEEE/CVF Conference on Computer Vision and Pattern Recognition*. 11506–11515.

[50] Yiyuan Zhang, Yuhao Kang, Sanyuan Zhao, and Jianbing Shen. 2022. Dual-Semantic Consistency Learning for Visible-Infrared Person Re-Identification. *IEEE Transactions on Information Forensics and Security* 18 (2022), 1554–1565.

[51] Yiyuan Zhang, Sanyuan Zhao, Yuhao Kang, and Jianbing Shen. 2022. Modality Synergy Complement Learning with Cascaded Aggregation for Visible-Infrared Person Re-Identification. In *European Conference on Computer Vision*. Springer, 462–479.

[52] Kuan Zhu, Haiyun Guo, Tianyi Yan, Yousong Zhu, Jinqiao Wang, and Ming Tang. 2022. Part-Aware Self-Supervised Pre-Training for Person Re-Identification. *arXiv preprint arXiv:2203.03931* (2022).

A APPENDIX

A.1 Effectiveness of CHPE

Table 5: Comparison in “mining RGB patches correlated to IR high-freq patches” versus “mining RGB patches with top-K high-freq responses” in CHPE.

Method	SYSU-MM01	
	R1 (%)	mAP (%)
Mining RGB patches correlated with IR high-freq patches	67.50	66.79
Mining RGB patches with top-k high-freq responses	67.03	65.38

To further verify the effectiveness of “CHPE”, we compare “mining RGB patches correlated to IR high-freq patches in CHPE” versus “directly mining RGB patches with top-K high-freq responses”. In Table 6, the Rank-1/mAP drops by 0.47%/1.41%. The main reason for the performance drop is that some RGB high-freq components are lost in the IR modality due to large differences in wavelength and scattering between RGB and IR modalities. Enhancing these RGB

patches introduces interference, which degrades performance. In contrast, although some RGB high-freq components are lost in the IR modality, there are always RGB patches highly correlated with IR high-freq patches. By computing patch-level similarity matrix with an EMA ViT, we can mine RGB patches correlated with sampled IR high-freq patches. These patches are less affected by variations such as wavelength and scattering than holistic images. Thus, enhancing the representation ability of these correlated high-freq patches benefits to effectively bridge the modality gap.

A.2 Effectiveness of Stop-gradient Operation

Table 6: Comparison in “w/. vs. w/o stop-gradient operation in Eq. (18) and Eq. (19).

Method	SYSU-MM01	
	R1 (%)	mAP (%)
w/o stop-gradient in Eq. (18) and Eq. (19)	71.92	70.59
w/ stop-gradient in Eq. (18) and Eq. (19)	70.73	68.27

The objective of the stop-gradient operation in Eq. (21) is to prevent cross-modal correlated high-frequency components from being disturbed by low-frequency ones in the global representation. As shown in Figure 1 of the manuscript, visually similar IR low-frequency patches can represent different semantics, causing feature representations to lose identity discrimination. The stop-gradient operation benefits the global representation f_g to capture discriminative and robust high-frequency components while mitigating low-frequency distractions. In contrast, the purpose of Eq. (18) and Eq. (19) is to capture comprehensive semantics of different modality instances. If a stop-gradient operation is applied, the propagation of gradient items between different modality instances will be reduced, which is not conducive to stable interactions between structural distributions of different modalities. To further verify it, we add a comparison between “with vs without stop-gradient in Eq. (18) and Eq. (19)”. From the result shown in the table below, we can see that the Rank-1/mAP drops by 1.19%/1.32%, which validates our analysis.

A.3 Visualization

Fig. 6 shows RGB-IR correlated high-frequency patches mined by Cross-modal High-frequency Patch Enhancement (CHPE). We can see that the selected patches mainly reflect pivotal high-frequency components of person images, such as heads, cloth textures, and human silhouettes. These patches are less affected by variations such as wavelength, pose, and background clutter than holistic person images, and thus are more robust to the modality gap.

Algorithm 1: The overall training procedure of ProtoHPE.

Input: Training datasets \mathcal{V}_{train} and \mathcal{R}_{train}
Output: The trained Part-based ViT Baseline.

```

1 for  $epoch=1$  to  $MaxEpochs$  do
2   for  $iter=1$  to  $MaxIters$  do
3     Sample a mini-batch  $\mathcal{V}_{\mathcal{B}} \subset \mathcal{V}_{train}, \mathcal{R}_{\mathcal{B}} \subset \mathcal{R}_{train}$ ;
4     // Part-based ViT Baseline
5     Enhance global and part representations by Eq. (2);
6     // Cross-modal High-freq Patch Enhancement
7     Mine RGB-IR correlated high-freq patches by Eq.
8     (4)-Eq. (8);
9     Enhance the representation ability of RGB-IR
10    correlated high-freq patches by Eq. (9);
11    // Multimodal Prototypical Contrast
12    Construct and dynamically update multimodal
13    prototypes by Eq. (10)-Eq. (12);
14    Use  $\mathcal{L}_{i2p}$  to reduce intra-modal variations of
15    instances belonging to the same identity;
16    Use  $\mathcal{L}_{p2p}$  to capture comprehensive semantics of
17    different modal instances;
18    Use  $\mathcal{L}_{p2p++}$  to prevent RGB-IR correlated high-freq
19    patches from being suppressed by low-freq ones;
20    // Overall objective function
21    Optimize the network by minimizing the overall
22    objective function in Eq. (22).
23  end
24 end

```



Figure 6: Visualization of RGB-IR correlated high-frequency patches mined by CHPE.

A.4 Overall Training Procedure

Algorithm 1 shows the overall training procedure of ProtoHPE. Let \mathcal{V}_{train} and \mathcal{R}_{train} denote the training datasets of visible and infrared images, respectively. At each episodic training iteration, the Part-based ViT Baseline takes the entire sequence (Eq. (1) of the manuscript) as input to enhance the discriminative power of both global and part representations. Subsequently, we utilize Cross-modal High-freq Patch Enhancement to enhance the representation ability of RGB-IR correlated high-freq patches. To obtain semantically compact and discriminative high-freq representations, we jointly utilize \mathcal{L}_{i2p} and \mathcal{L}_{p2p} , which facilitates the aggregation of representations belonging to the same identity. Furthermore, we use \mathcal{L}_{p2p++} to prevent RGB-IR correlated high-freq components from being suppressed by low-freq ones when taking the entire sequence Eq. (1) as input during network optimization. By virtue of \mathcal{L}_{p2p++} , ProtoHPE is only necessary during training and can be removed during inference. Finally, we optimize ProtoHPE by minimizing the overall objective function in Eq. (22). During inference, only the Part-based ViT Baseline is necessary and our ProtoHPE can be removed, thus bringing no additional complexity.

Received 20 February 2007; revised 12 March 2009; accepted 5 June 2009